Space Science and Engineering Center
University of Wisconsin–Madison

A REPORT
OF THE
SEVERE WEATHER PROGRAM
FOR THE PERIOD
1 SEPTEMBER 1994 TO 31 AUGUST 1995

A REPORT from the

COOPERATIVE INSTITUTE FOR METEOROLOGICAL SATELLITE STUDIES

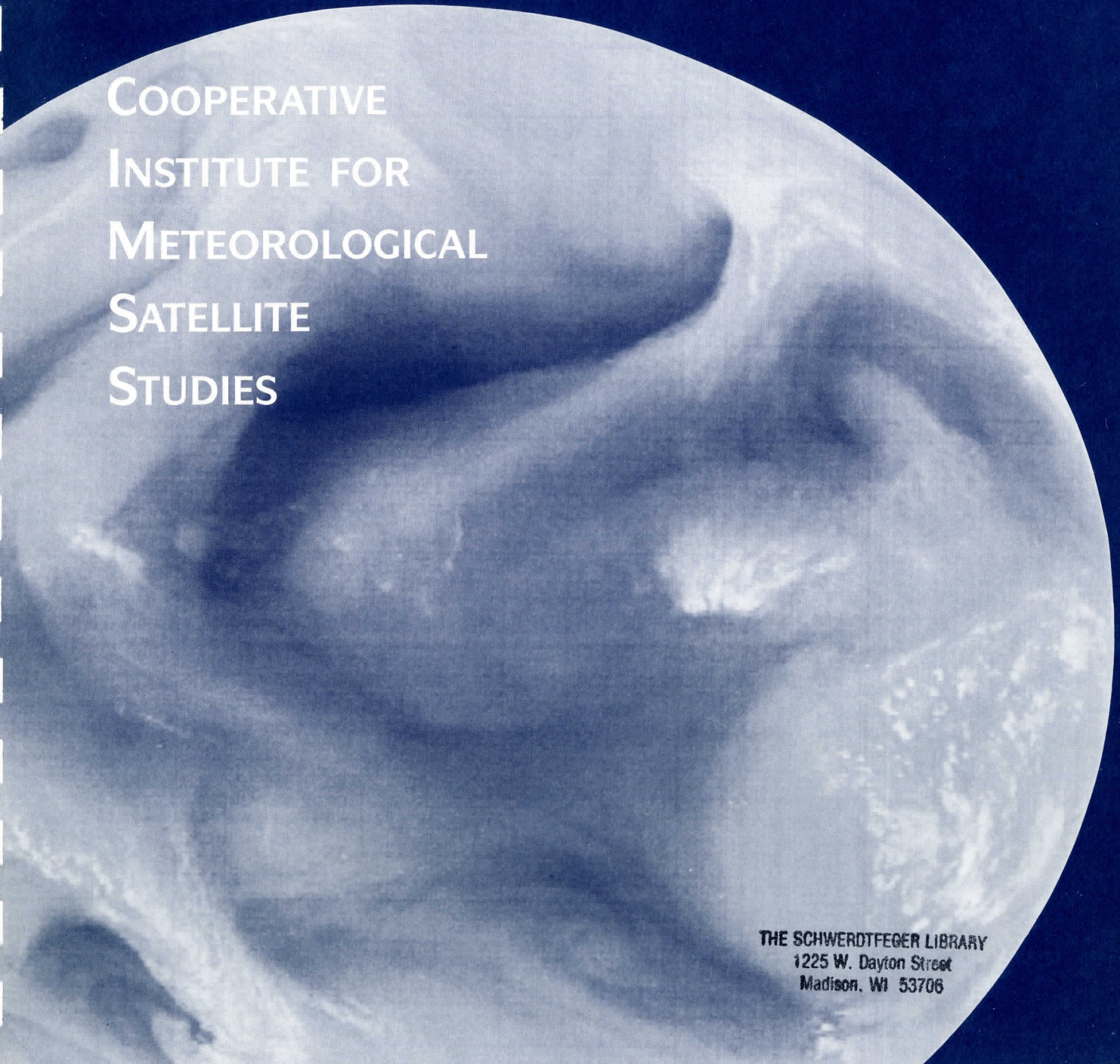

A REPORT
OF THE
SEVERE WEATHER PROGRAM
FOR THE PERIOD
1 SEPTEMBER 1994 TO 31 AUGUST 1995

Submitted by

Cooperative Institute for Meteorological Satellite Studies
Space Science and Engineering Center (SSEC)
at the University of Wisconsin-Madison
1225 West Dayton Street
Madison, Wisconsin 53706
(608) 263-7435

Christopher M. Hayden
Chief, SDAB
Principal Scientist

William L. Smith
Director, CIMSS
Principal Investigator

Anthony J. Schreiner
Associate Researcher
Program Manager

TABLE OF CONTENTS

I. INTRODUCTION

This report describes the work done on Research Grant #NA17ED0427-01 during the period from 1 September 1994 through 31 August 1995. The purpose of this report is to give a brief summary of the various and diverse projects being supported during the contract period. Sections III and IV summarize the scope of the research work and list references, respectively. The reference section includes all published papers and conference reports resulting from this research work (indicated by an * and in **bold type**) plus the cited articles in the RESULTS section.

The primary objectives of this grant are twofold. The first objective is the use of remote sensing data to study the evolution of the storm environment. This includes investigations of the moisture budget and cloud conditions over meso to cyclone periods. The second objective is the examination of the dynamical and statistical evolution of the storm environment through use of remote sensing data assimilated into numerical weather prediction models. The program is thus directed to end-to-end application of satellite data to culminate in improved application of satellite data to the severe weather forecasting problem.

The main research areas covered in Section II of this report are:

- The evolution of and improvements to the CIMSS Regional Assimilation System (CRAS) model. Continued streamlining and additional applications are being developed for the CRAS.
- The development of satellite-derived products using the VISSR Atmospheric Sounder (VAS) and the GOES-8 Sounder and Imager radiance information. Areas of concentration continue to be application of derived-products for the purpose of understanding and forecasting the weather, assimilation into numerical prediction models, and, through comparison to high spatial and temporal CLASS radiosondes, verification of the remotely sensed temperature and moisture soundings.
- Derivation of an image and gridded cloud product using the GOES-8 Sounder data. With the advent of the Global Energy and Water Cycle Experiment (GEWEX), there is a requirement for an hourly gridded cloud product over the continental United States.

II. RESULTS

A. Initializing Clouds and Moisture using the GOES-8 Sounder. Contributed by Robert M. Aune

Operational numerical weather prediction centers are beginning to incorporate more sophisticated cloud prediction schemes in their prediction models (Zhou and Black 1994). Real-time cloud scale predictions of particular interest to the aviation and agricultural communities, the tourism industry, and the military will soon be available on a regular basis. The accurate prediction of clouds in mesoscale forecast models will require some type of cloud initialization. High spatial and temporal resolutions will be required. Problems concerning the spin-up of cloud and precipitation in the first 3 hours of a forecast can be significant. The sounder on the new GOES-8 satellite can provide cloud and moisture observations that models can use (see Menzel and Purdom 1994). An algorithm to retrieve cloud-top temperature and pressure from the sounder has been developed and verified by Schreiner et al., (1993). Observations are available at one hour intervals over the sounders field of view. The retrievals are computed using a subset of the 19 spectral channels, at a horizontal resolution of approximately 50 km (5 x 5 pixels, 10 km FOV). Retrieved parameters include cloud-top pressure and temperature, and effective emissivity which is the ratio of the cloud emissivity including the cloud fractional coverage.

To build a 3D cloud field using only cloud-top pressure observations requires the use of additional information to specify the depth of the cloud and the vertical distribution of cloud water mixing ratio. The vertical profile of water vapor mixing ratio, collocated with the cloud, may also need to be modified so that the model physics will support the existence or absence of a cloud. To accomplish this a number of schemes were tested. The most successful approach to date is summarized as follows:

1) The observed cloud-top pressures are analyzed to the model grid (80 km). For this experiment a zero field first guess was used. Predicted cloud water fields from a previous forecast have also been used with good success.
2) Model grid points containing clouds are identified. An effective cloud emissivity fraction below 50% is considered clear. This threshold may vary with model resolution.
3) A cloud base is computed by searching for dry layers below the cloud top. The updated (using rawinsonde dew points) model moisture analysis is used. If a suitable layer exists, a parabolic cloud water profile is computed following Wu et al. (1995). Maximum cloud depths are parameterized as a function of the cloud-top height. Vertical motions generated by the models vertical normal-mode initialization have been used to identify areas of active cloud production with good success.
4) The initial mixing ratio profile is adjusted to support the presence of cloud water. Because a specified relative humidity profile is used to control the growth and dissipation of cloud water in the model physics, the mixing ratio must be modified or the initialized clouds quickly disappear.

Implicit in the GOES-8 cloud data sets are clear sky observations. These are useful when assimilating cloud data in a 4D mode for controlling the over-production of clouds and identifying deficiencies in a particular forecast. In addition, precipitable water retrievals are available from the same

radiance data set over clear areas. In this work, total precipitable water retrievals were used in clear areas to adjust the water vapor mixing ratio using the method described by Aune (1994).

The cloud initialization was implemented in the CRAS pre-forecast subsystem. The CRAS is a real-time, hydrostatic, mesoscale analysis/prediction system (Raymond et al. 1995, Wu et al. 1995, and Diak et al. 1992). The system provides a software platform for the development and testing of satellite data and assimilation algorithms. The 80 km version of the CRAS was implemented on 1 February 1993 and runs daily in real-time. An analysis is produced using rawinsondes, surface reports and AVHRR SST's at synoptic times and geopotential heights, precipitable water and cloud motion winds from the GOES-8 satellite. NGM analysis fields are used for background. The forecast is nested in NMC's Aviation forecast and is run out to 48 hours. Retrievals from the GOES-8 sounder are currently being used in the daily 00 UTC forecast. The model predicts cloud liquid water mixing ratio using an approach similar to Kessler (1974). Raymond et al. (1995) gives a description of the cloud water parameterization.

The impact of initializing the cloud water field is determined by comparing forecasts with initialized clouds (INCLD) to a parallel forecast with zero initial cloud water (NOCLD). Verification of 12 hour forecasted temperatures at 925 hPa, 850 hPa, and 700 hPa against rawinsonde temperatures consistently show a slight reduction in RMS and bias. Table 1 shows the verification statistics for a 12 hour temperature forecast valid at 1200 UTC on 1 September 1995. Although the improvement here is small it is consistently positive from day to day. Larger improvements have been observed. An objective verification of forecasted cloud fields is more difficult. A subjective comparison is routinely conducted using IR images derived from forecast data sets.

TABLE 1

LEVEL	NOCLD	INCLD	NOCLD	INCLD
hPa	RMS	RMS	BIAS	BIAS
925 T	1.48	1.46	1.18	1.14
850 T	1.42	1.40	.88	.85
700 T	1.53	1.51	1.02	.99

A verification of 24 hour accumulated precipitation is shown in Figures 1, 2 and 3. Figure 1 shows the 24 hour accumulated precipitation (mm) from the NOCLD forecast, Fig. 2 the INCLD forecast, and Fig. 3 shows the corresponding rain gauge observations. The initialization of the cloud field and the inclusion of total precipitable water in clear sky areas has increased the amount of precipitation along a line extending northeast to southwest in western Virginia and North Carolina. This increase appears to agree more favorably with the rain gauge observations.

The scheme described above is being tested on a daily basis. Verification statistics are consistently positive. A modest positive impact on the precipitation forecasts has been observed in a number of cases. Further experimentation is needed to see if the model's cloud parameterization can be modified to improve cloud water predictions as verified against GOES-8 observations. An improved

algorithm that uses information from the model background fields to identify areas of active cloud growth and decay is currently being implemented. Statistical comparisons between the model variables and the GOES-8 retrievals are also being conducted.

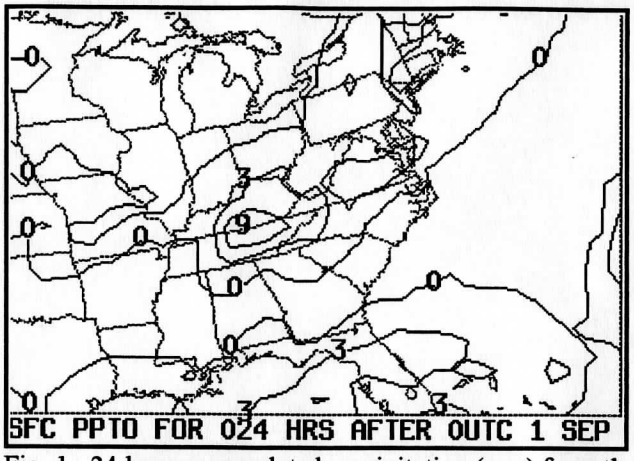

Fig. 1. 24 hour accumulated precipitation (mm) from the NOCLD forecast valid 0000 UTC 02 September 1995.

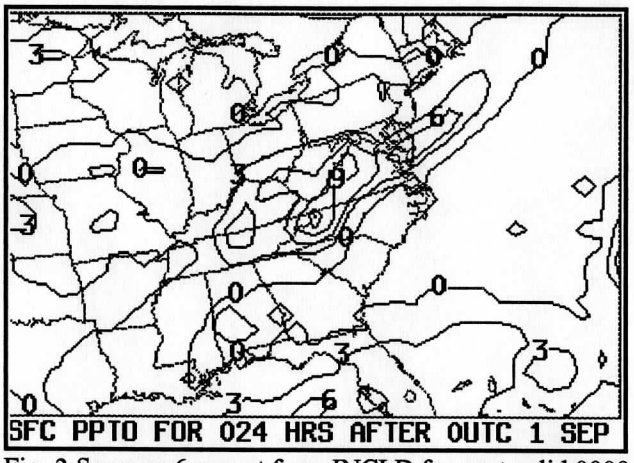

Fig. 2 Same as 6 except from INCLD forecast valid 0000 UTC 2 September 1995.

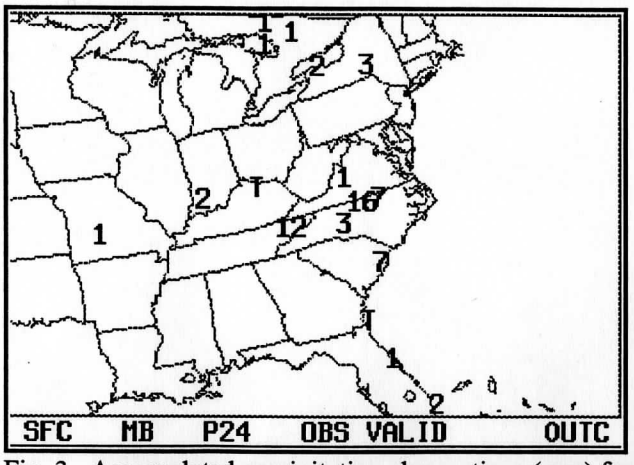

Fig. 3. Accumulated precipitation observations (mm) from synoptic rain gauge network for the period ending 0000 UTC 2 September 1995.

B. A K-Theory Turbulence Parameterization Based on Nonlocal Mixing Probabilities.

Contributed by William H. Raymond and Robert M. Aune.

Many schemes have been designed to estimate the eddy diffusion coefficient K in grid-scale K-theory turbulence parameterizations (Stull 1988). However, accurate twenty-four hour forecasts of near surface atmospheric variables remain elusive and usually contain errors larger than those found at mid-atmospheric levels. To help in this regard a new K- theory turbulence parameterization has been introduced. In our study we make the K's proportional to mixing probabilities that are computed from a nonlocal formulation of the turbulent kinetic energy equation. These probabilities range in values between one and zero which identifies the upper and lower limits of complete mixing and no mixing, respectively. These spatial and time variations in K (proportional to mixing probabilities) reflect the complexity of the turbulence. In comparisons with traditional K-theory methods we find that our K-theory turbulence parameterization gives superior forecasts in the boundary layer. Results are presented in Fig. 1 showing the 850 hPa root mean squared temperature error for one 48 hour forecast beginning at 0000 UTC 25 April 1994. Based on rawinsonde measurements the nonlocal approach clearly produces smaller root mean squared errors.

Our computationally-fast boundary layer parameterization has been installed in the operational forecasts that are run twice daily at CIMSS. This mixing scheme also includes a viscous layer so that the surface temperature can experience realistic temperature ranges. This improved forecast tool will assist us in future data assimilation experiments.

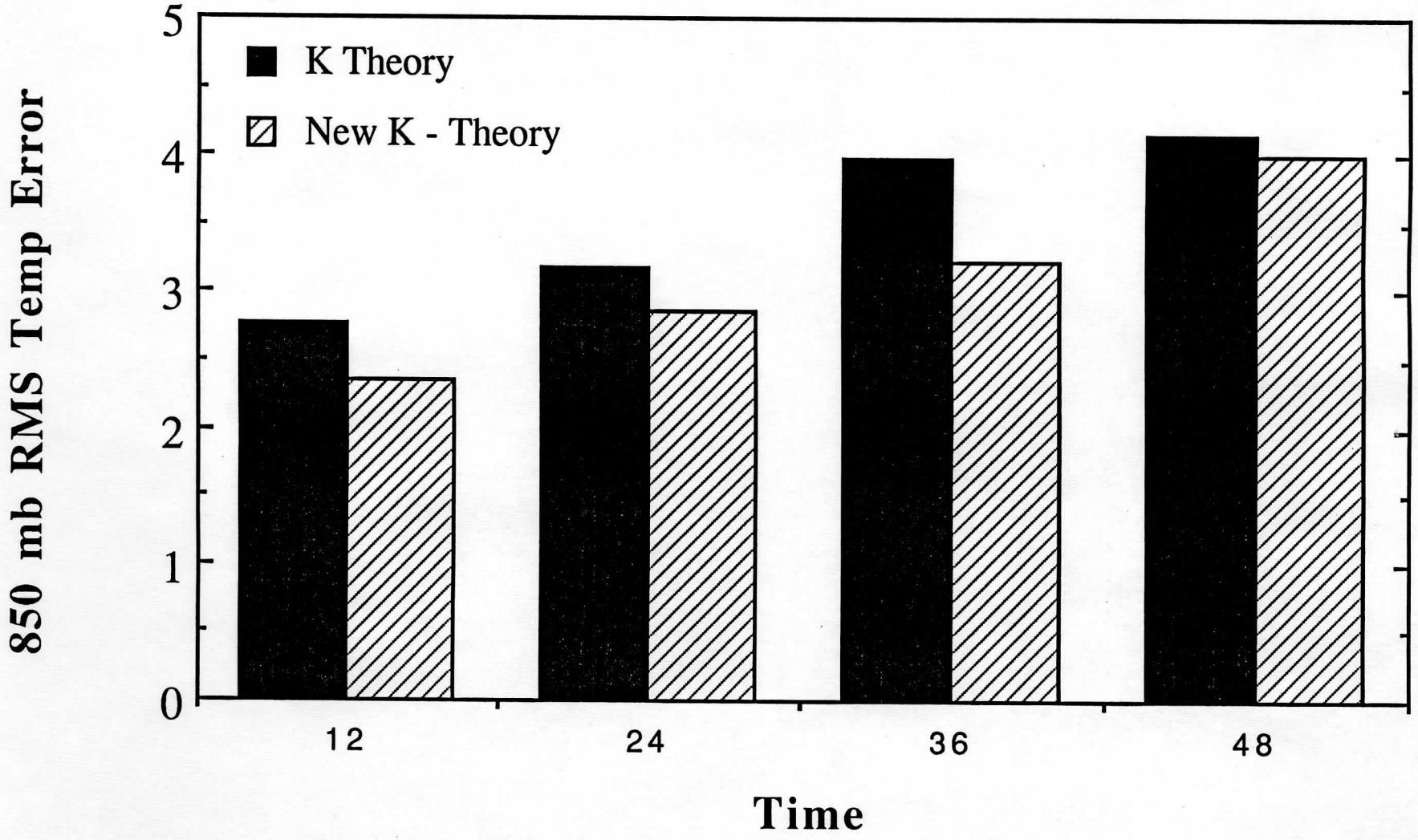
850 mb RMS Temp Error
5
4
3
2
1
0
K Theory
New K - Theory
12
24
36
48
Time

C. Variational Assimilation of Satellite Observed Gradient Wind Data. Contributed by Xiaohua Wu and Christopher M. Hayden.

A well-documented deficiency of temperature soundings derived from satellites is a regional, weather system dependent bias caused by the limited vertical resolution of the radiance measurements. Because of this, a number of investigators have sought to use the data as horizontal temperature gradients rather than as absolute measurements (Cram and Kaplan; 1985, Aune et al., 1987). At NESDIS, radiance data from the GOES VAS has been routinely processed in the form of "gradient winds" since 1992, offering the modeling community the opportunity of using temperature gradient information in this form. These gradient winds have been shown to be useful in defining hurricane track forecasting, and, after a period of testing, were added to the operational data base at the National Weather Service Environmental Modeling Center in February 1994. However, use of these data as "winds" when they actually represent thermal gradients is clearly not optimal, and the purpose of this research was to investigate a variational technique for assimilating the gradient winds into the geopotential analyses of the CRAS.

The assimilation technique is a modified version of the variational 'field by information blending" technique used in the CRAS. The independently analyzed fields of geopotential and geopotential gradient are combined using the calculus of variations. The basic principle of variational analysis is to minimize differences between the objective analyzed values and the newly adjusted values in a least-squares sense, subject to one or more dynamic constraints. In this study, one constraint used is to match the gradients derived from VAS gradient wind data and the model analyzed values; another is a vertical coupling constraint on the adjustments, which ensures the adjusted geopotential satisfy the hydrostatic relationship. The error functional to be minimized is

$$I = \int_x \int_y \int_p \{A(\phi - \tilde{\phi})^2 + B[(\nabla_x \phi - \nabla_x \hat{\phi})^2 + (\nabla_y \phi - \nabla_y \hat{\phi})^2] + C(\nabla_p \phi - \nabla_p \tilde{\phi})^2\} dxdydp \qquad (1)$$

where $\tilde{\phi}$ is the first-guess (from CRAS analysis) geopotential, ϕ is the adjusted geopotential, $\nabla_x \hat{\phi}$ and $\nabla_y \hat{\phi}$ are the horizontal geopotential gradients in the x and y directions derived from VAS gradient wind data and ∇_p is the vertical gradient. A, B, C are 3-dimensional reliability weights for the independently analyzed geopotential, gradient fields and geopotential thickness. They are determined on the basis of data density fields produced during the CRAS analyses, latitude- and level-varying standard deviation parameters, and externally specified tuning parameters. In this way one can ensure, for example, that the blended geopotential fields reflect a greater weight to the wind data in low latitudes, and to the thickness at higher latitudes.

Sensitivity tests were performed with simulated geopotential and gradient networks to verify the potential of the method and to investigate the effect of spatial densities. As expected, the method was shown to work, and results were improved at greater data densities. Under specific circumstances, the resultant geopotential fields analyzed with the gradient winds were as effective (in simulation forecasts) as those analyzed with simulated temperature observations.

Tests with real gradient winds were performed for 20 test cases taken from January, 1994, examined in terms of the accuracy of 48 hour numerical forecasts with the CRAS. Forecasts were initiated with three analyses: a conventional data set using rawinsondes only (RAOBRUN); a set augmented with VAS temperature retrievals (RAOB+VAST), and a set augmented with VAS gradient winds (RAOB+VASWD). The vertically averaged temperature error of the 12, 24, 36 and 48 hour forecasts is given in Fig. 1, as verified against the conventional CRAS analysis over the U.S. As indicated in the figure, we found a small positive impact associated with the use of the VAS data either as temperature or gradient winds. The use of the gradient data had a slightly more positive impact on geopotential height forecasts, especially at the upper levels.

A manuscript describing this research in more detail has been submitted to the Monthly Weather Review.

Figure 1. Vertically averaged RMS. temperature errors (^{0}C) for twenty forecast experiments using rawinsondes (RAOBRUN); rawinsondes plus VAS temperature retrievals (RAOB+VAST); rawinsondes plus VAS gradient winds (RAOB+VASWD).

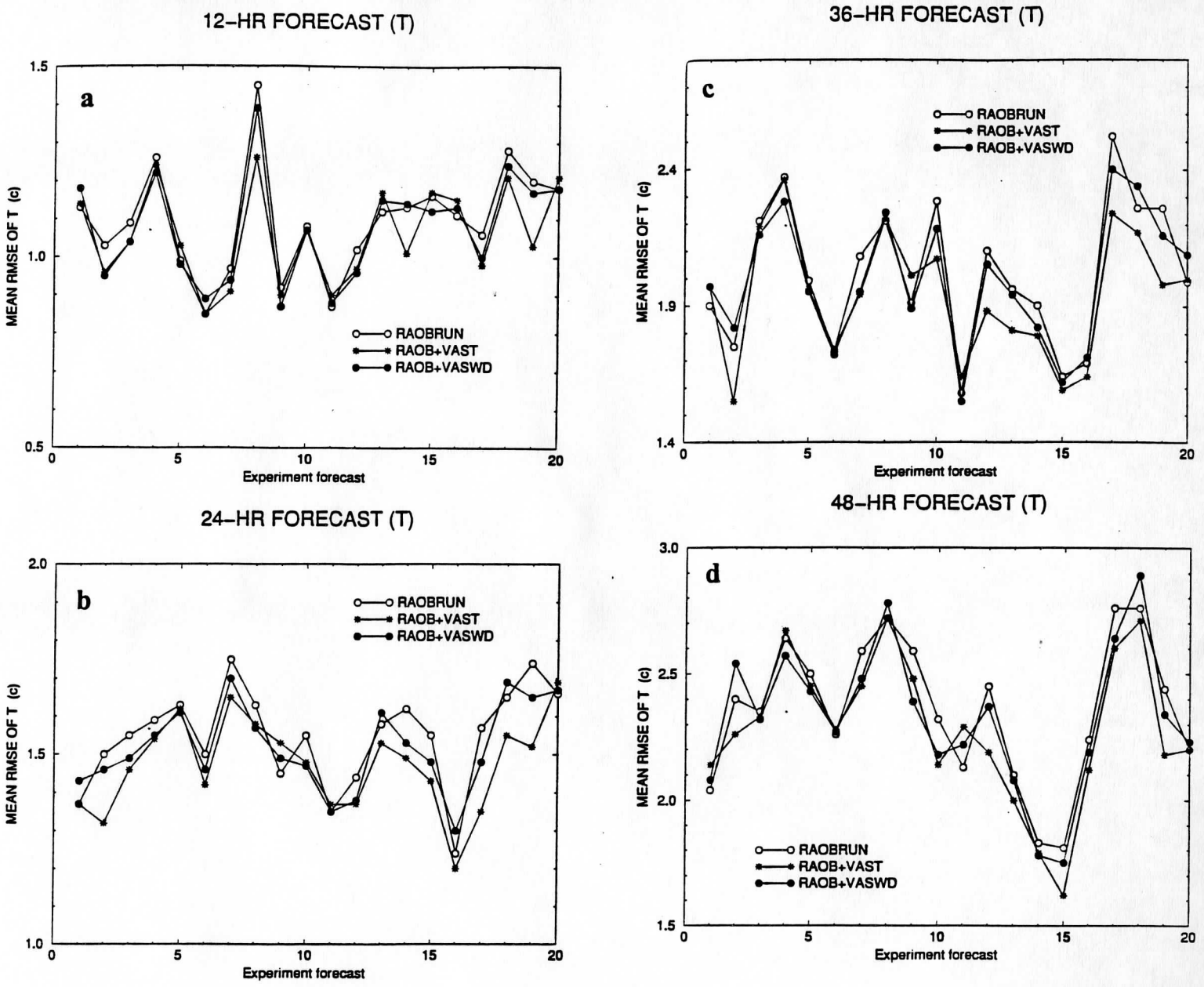
12–HR FORECAST (T)
a
MEAN RMSE OF T (c)
Experiment forecast
RAOBRUN
RAOB+VAST
RAOB+VASWD
36–HR FORECAST (T)
c
MEAN RMSE OF T (c)
Experiment forecast
RAOBRUN
RAOB+VAST
RAOB+VASWD
24–HR FORECAST (T)
b
MEAN RMSE OF T (c)
Experiment forecast
RAOBRUN
RAOB+VAST
RAOB+VASWD
48–HR FORECAST (T)
d
MEAN RMSE OF T (c)
Experiment forecast
RAOBRUN
RAOB+VAST
RAOB+VASWD

FIG. 1

D. Evaluation of GOES-8 Sounding Products during the VORTEX. Contributed by Robert M. Rabin and Gary S. Wade.

An evaluation of the accuracy of GOES-8 sounding products by comparison with CLASS soundings during VORTEX (Verification of the Origins of Rotation in Tornadoes Experiment) is planned. The evaluation process began with on-site assistance of VORTEX operations by SDAB and CIMSS personnel during the spring of 1995. Real-time derived image products were used by forecasters during operations of the field experiment. Comparison of satellite derived and in-situ CLASS soundings is now underway. The high temporal and spatial coverage of these soundings provide a unique opportunity to evaluate the utility of the satellite data in depicting atmospheric moisture patterns associated with convective storm development. Efforts have begun to evaluate the impact of satellite sounding data on forecasts of deep convection through VORTEX case studies with the CRAS model.

A list of case study days is as follows:

Initial Case Study Days from VORTEX

	Date	Events of Interest
1.	22 May 1995	Non-tornadic supercell in Texas Panhandle with very distinct dry line.
2.	1 June 1995	Localized severe weather in Norman, OK area not anticipated.
3.	2 June 1995	Large tornadic storms in far western Texas Panhandle (Friona and Dimmitt, TX) along outflow boundaries.
4.	8 June 1995	Large tornadic storms in eastern Texas Panhandle (Pampa and Allison, TX).

For cases 1, 3, and 4 numerous extra upper air data were collected (including mobile CLASS radiosondes); these available data will be compared with the three hourly temperature/moisture retrievals from the GOES-8 Sounder radiance data. A second method to evaluate the Sounder retrievals will be to use them in an assimilation experiment with the CIMSS Regional Assimilation System (CRAS) model, employing three hourly updates, and comparing with a control run. The three hourly Sounder retrieval data sets will be processed using the latest version of the temperature/moisture algorithm. The first case for this approach will be from 1 June 1995.

The hourly Derived Product Imagery (DPI) provide depictions of total moisture, atmospheric stability, and surface skin temperature with good temporal and horizontal resolution in clear areas. The ability of the DPI to provide continuity to the evolution of the observed pre-convective environment is to be verified. Likewise, the hourly DPI will be processed in a non real time mode.

E. Upper Tropospheric Humidity Variations. Contributed by Xiangqian Wu, W. Paul Menzel, Christopher M. Hayden, Steven J. Nieman, and Christopher S. Velden.

The upper tropospheric relative humidity (UTH) has been retrieved twice a day (near 00 UTC and 12 UTC) from METEOSAT-3 and GOES-7 water vapor images, from July 1994 to June 1995 (METEOSAT-3 was decommissioned at the end of May 1995). Our preliminary analysis of this product reveals interesting features of annual, interannual, and diurnal variations.

Figure 1 shows the monthly mean UTH at 00 UTC for every other month over the 12-month period. The inter-tropical convergence zone (ITCZ) in the Atlantic and Eastern Pacific Oceans appears in Fig. 1 as a narrow band of high values of UTH. It is stronger and farther north in July than in January. Similar convection features and their annual variation are evident over the Amazon, Central America, and the Florida Peninsula.

A unique feature of the upper tropospheric water vapor distribution is its ability to identify the location and strength of subsidence in the upper troposphere, shown as area of low UTH values. The subsidence forms a crescent around the west and north of the South American continent in winter (January-March), corresponding to the convection center over the Amazon Basin. In summer (July-September), it becomes elongated south to the Equator in the Eastern Pacific Ocean, completing the Hadley cell with the ITCZ.

In March 1994, there was a narrow band of low values in the UTH field over the Equator in the Eastern Pacific Ocean. It was best defined near the South American coast, becoming weaker gradually towards the center of the ocean. This feature is suggested to be a signature of a split ITCZ, with a band of subsidence marked by the low UTH and two bands of weak convection on its flanks. In March 1995, this feature is barely detectable.

The twice daily observations of the UTH offers us limited opportunity to study its diurnal variability. Figure 2 presents the monthly mean differences, for the same months as in Fig. 1, between the UTH at 00 UTC and the UTH at 12 UTC. For this part of the world, the local time is early (west) to late (east) afternoon at 00 UTC and early to late morning at 12 UTC. Figure 2 shows that convection centers have large diurnal variation; regions of subsidence have almost no diurnal variation. For example, in July the difference is large and positive around the Caribbean Sea, but the difference is nearly zero over the Amazon basin. In January, the reverse is true.

Comparing to its counterpart over the land, convection over the oceans has weaker diurnal variation. The well-defined South Pacific Convergence Zone in November 1994, for example, shows little diurnal variation. The diurnal variation of ITCZ is more visible, indicating that more water vapor has been transported to the upper troposphere by the afternoon, especially when the ITCZ is vigorous (July).

This data set also sheds lights on the inter-calibration of the data from two satellites. In March 1994, it was found that the UTH from METEOSAT-3 appeared drier than that from GOES-7. This can be seen from the upper panel of Figure 3. In March 1994 and over a region viewed by both satellites with similar angles, there are more pixels with smaller UTH values and less pixels with larger UTH values for METEOSAT-3 (solid line), compared with GOES-7. If that difference were attributed to the difference in spectral characteristics of the water vapor channels on the two satellites, it would imply that relative humidity increases with height in the upper troposphere. So we suspected that the calibrations of the two satellites were inconsistent with each other. For the later half of 1994, the difference between the UTH derived from the two satellites disappeared (lower panel of Fig. 3). However, the right column of Fig. 1 suggests that similar difference reappeared in 1995, especially in March. Unfortunately, GOES-7 had been relocated by then, making it impossible for the inter-satellite comparison like those in Fig. 2. However, evidence so far suggests that the wet bias of GOES-7 relative to METEOSAT-3 is a seasonal phenomenon.

Figure 1: Monthly mean UTH by GOES-7 (left) and METEOSAT-3 (right) for selected months.

Figure 2: As Figure 1, but for the monthly mean differences of UTH between 00 UTC and 12 UTC.

Figure 3: Frequency of pixels having certain value of UTH within an area viewed by both GOES-7 and METEOSAT-3. The "kinks" at UTH=5%, 15%, 30%, and 60% were due to the log-linear interpolation of the UTH between these values.

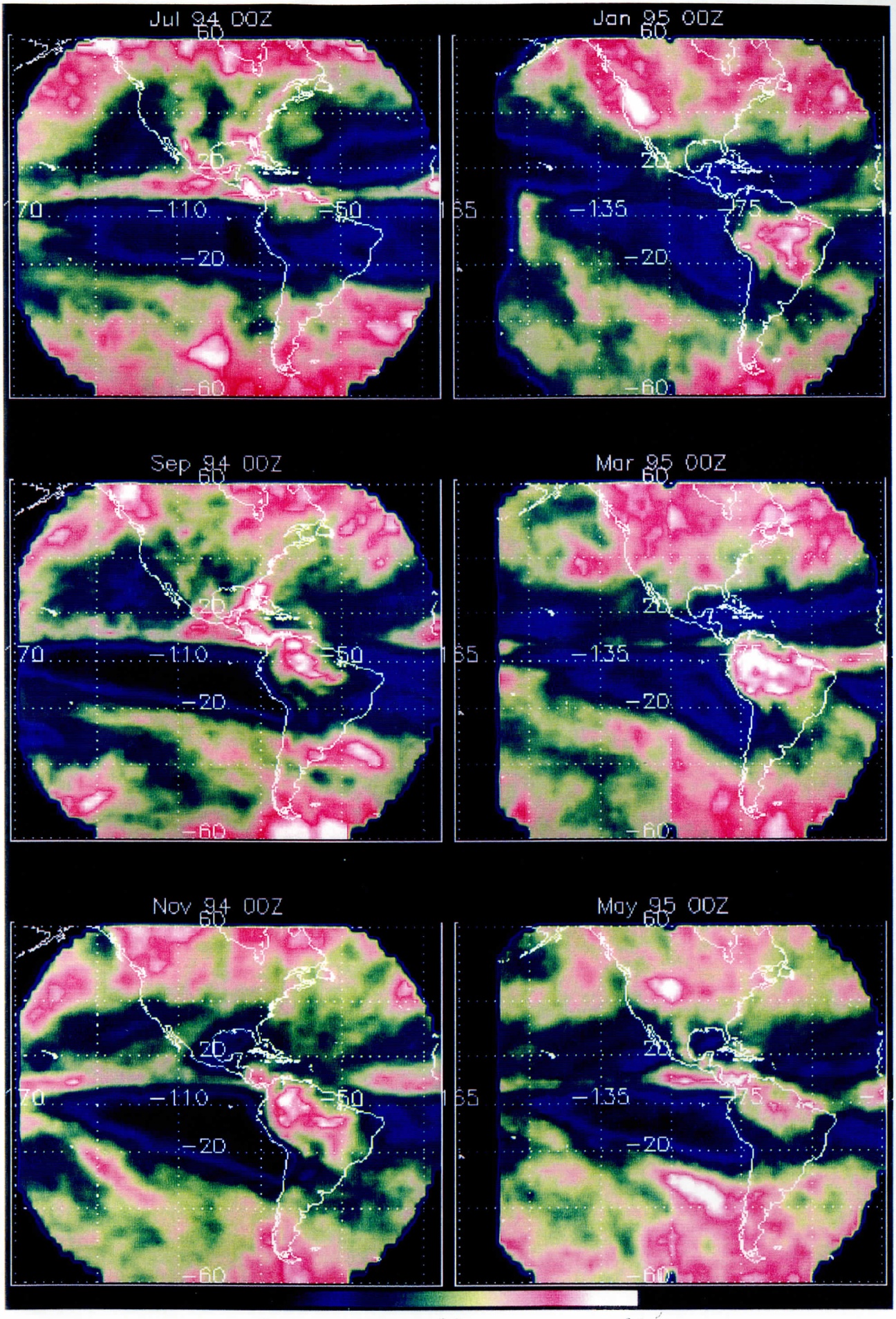
Jul 94 00Z
Jan 95 00Z
Sep 94 00Z
Mar 95 00Z
Nov 94 00Z
May 95 00Z
60
20
-110
-50
-20
-60
-135
-75
0
40
80

Fig. 1

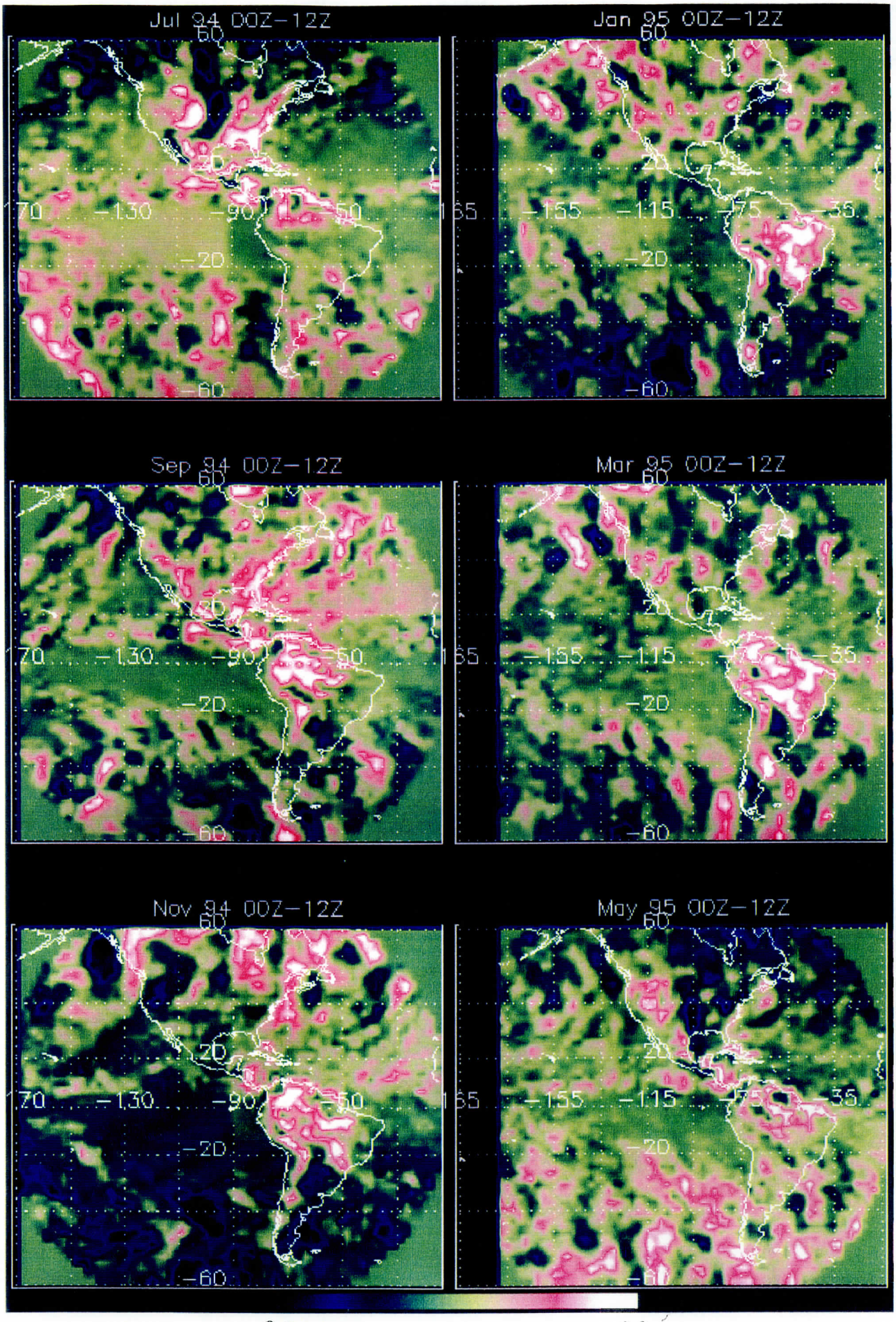
Jul 94 00Z–12Z
Jan 95 00Z–12Z
Sep 94 00Z–12Z
Mar 95 00Z–12Z
Nov 94 00Z–12Z
May 95 00Z–12Z
60
20
70
130
90
50
165
155
115
75
35
20
60
-20
0
20

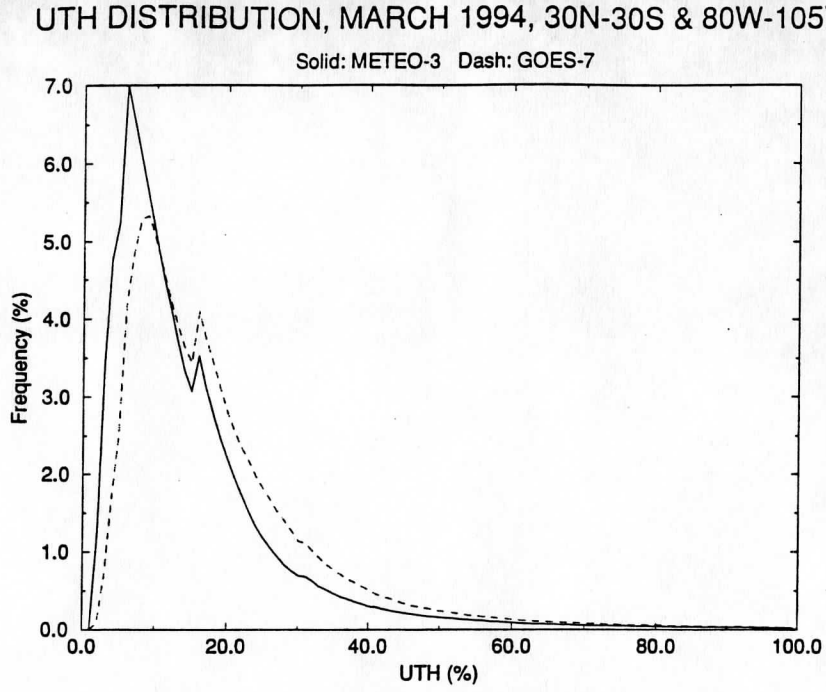
UTH DISTRIBUTION, MARCH 1994, 30N-30S & 80W-105W
Solid: METEO-3 Dash: GOES-7
Frequency (%)
7.0
6.0
5.0
4.0
3.0
2.0
1.0
0.0
0.0
20.0
40.0
60.0
80.0
100.0
UTH (%)

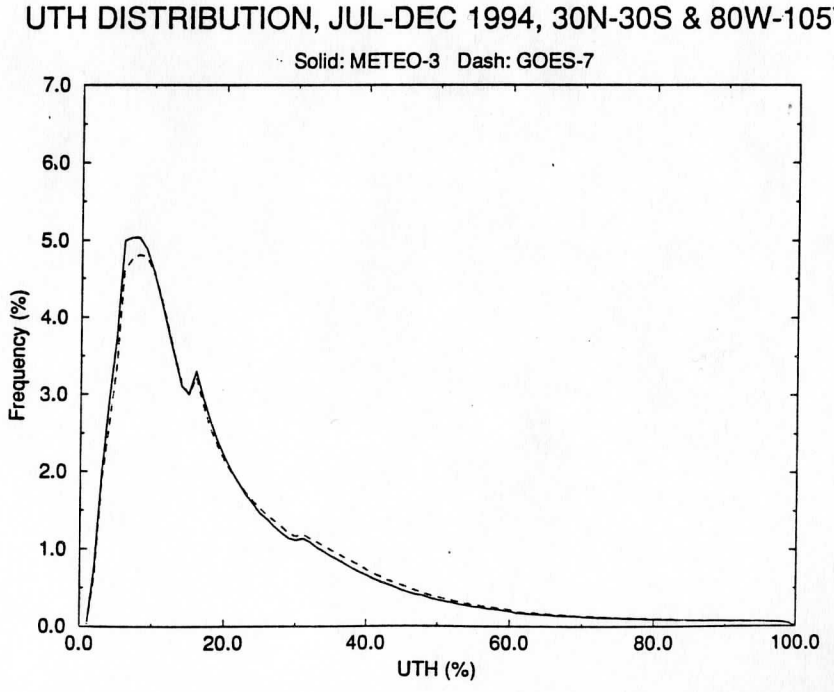
UTH DISTRIBUTION, JUL-DEC 1994, 30N-30S & 80W-105W
Solid: METEO-3 Dash: GOES-7
Frequency (%)
7.0
6.0
5.0
4.0
3.0
2.0
1.0
0.0
0.0
20.0
40.0
60.0
80.0
100.0
UTH (%)

FIG. 3

F. Evaluation of the GOES Surface Skin vs. Air Temperature Model. Contributed by Christopher M. Hayden.

For several years the Severe Weather Program has supported research in formulating an empirical model relating the skin vs. air temperature difference as a function of the surface air temperature, dew point, length of day, and solar zenith angle. The model is included in the operational processing suite for the GOES cloud clearing algorithm. The derived skin temperature from the model is compared with corrected window channel estimates as one of the basic tests to determine clear fields-of view (the other being a visible radiation check). During the past year we have had occasion to consider the accuracy of this model, and it has been discouraging. Three hourly examples of the comparison between the model estimate of skin temperature and the final, retrieved skin temperature derived from GOES-8 measurements are provided in Fig. 1. Three hourly examples of a similar comparison between simply the surface air temperature and the retrieved skin temperature are shown in Fig. 2. It is apparent from a comparison of the figures that the model generally overpredicts the skin/air difference during the night, especially at lower temperatures. Radiational cooling anticipated is much too strong. During the hot part of the day, especially 18 and 21 UT, the model fails completely; the modeled "cooling" of the skin is clearly beginning too soon. In all cases the unmodified surface air temperature appears to be at least as good a predictor of the skin temperature as the modeled estimate, excepting, perhaps, a couple of outliers at 12 UT in Fig. 2.

It appears that a better "model" would be a simple linear regression as shown by the solid lines in Fig. 3, or perhaps better yet a multiple linear regression. These options have been investigated using as predictors the surface air temperature, the local zenith angle, the solar zenith angle and longitude. The result for the multiple linear regression is shown in Fig. 3. Statistics for the linear regression are given in Table 1, and a statistical analysis of the accuracy of the three methods is given in Table 2.

Table 1 shows that the surface air temperature dominates as a predictor as would be anticipated. The example shown is for 18 UT, but the same is true at all time periods. Table 2 shows that the rms error in the skin temperature estimate is greatly reduced by using regression instead of the model (from 5.6K to 1.5K). There is only a slight advantage in including extra predictors beyond the surface air temperature.

The largest effect of substituting the regression model for the physical model in the GOES processing occurs in the pre-dawn hours. This is most clearly seen in animated sequences of Derived Product Imagery where the cloud continuity is clearly improved. Because the physical model predicted too large a nocturnal cooling, some low cloud scenes were not properly identified. This was also reflected in the accuracy of the GOES temperature/moisture retrievals which improved with the correct cloud interpretation.

Table 1. Multiple regression results for predicting surface skin temperature from surface air temperature (Ta), solar zenith angle (SZ), local zenith angle (LZ), and longitude (Lon). Sample size, standard deviation (σ), explained variance (ev) and standard error of estimate (ee), and coefficients are shown. Sample period is 18 UT.

Sample	σ	ev	ee
656	7.11	.96	1.48

parameter	Ta	SZ	LZ	Lon
Coefficient	.991	.-.125	.115	.006

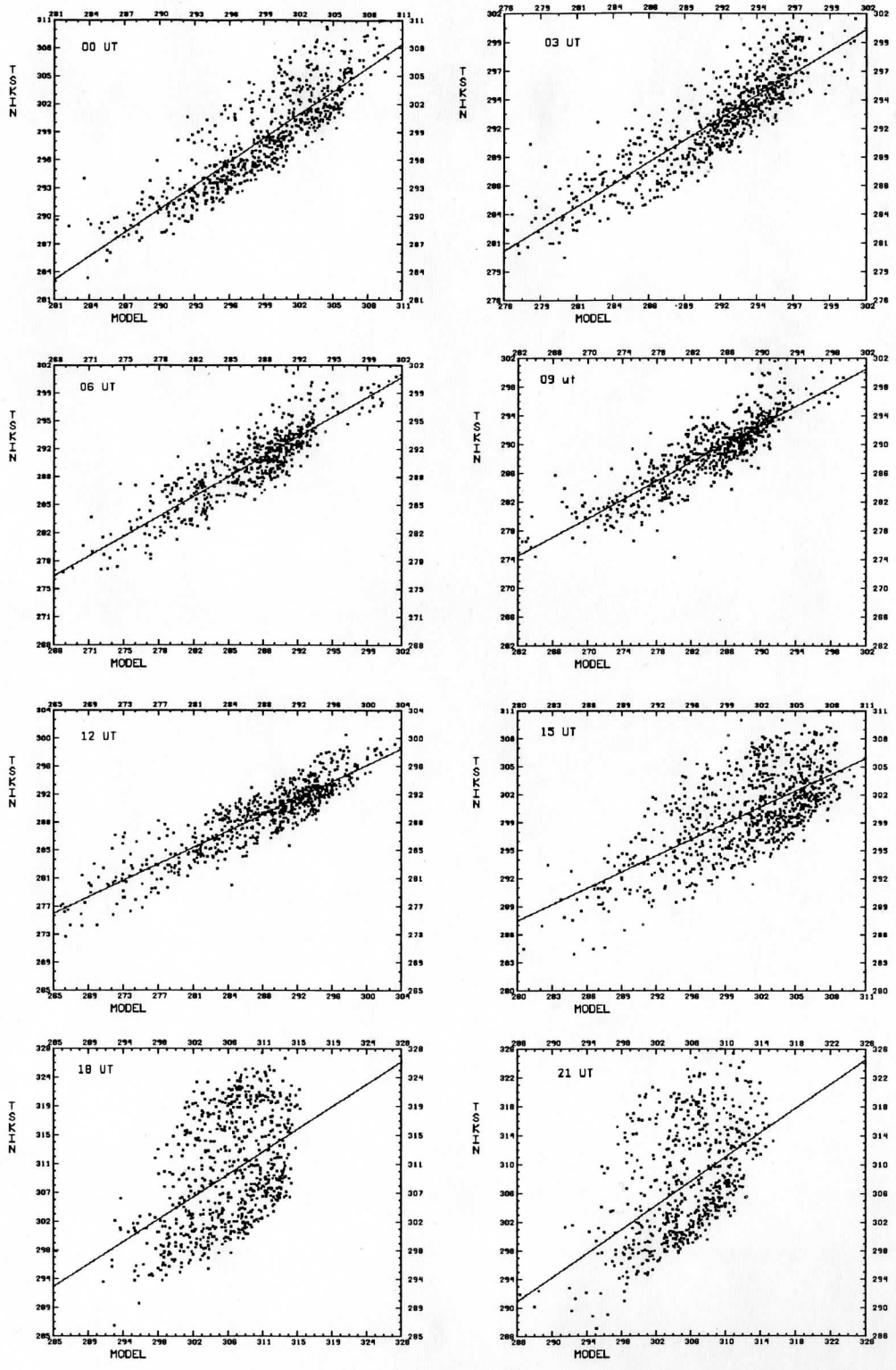

Fig. 1. Surface skin temperature as obtained from GOES-8 retrievals vs. value predicted with empirical model. Six time periods through the day are shown. Values are K.

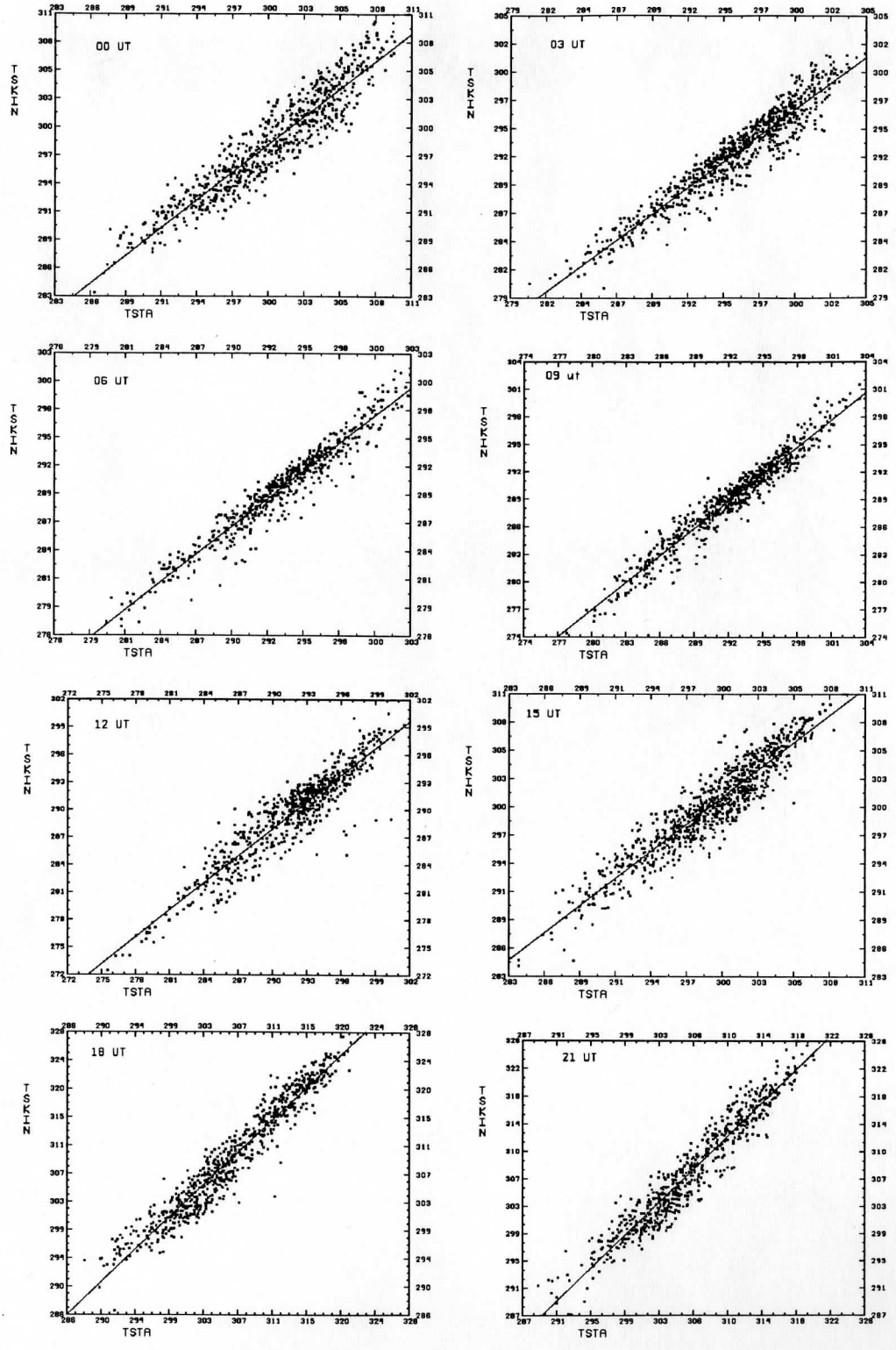

Fig. 2. Surface skin temperature as in Fig. 1 vs. surface air (TSTA).

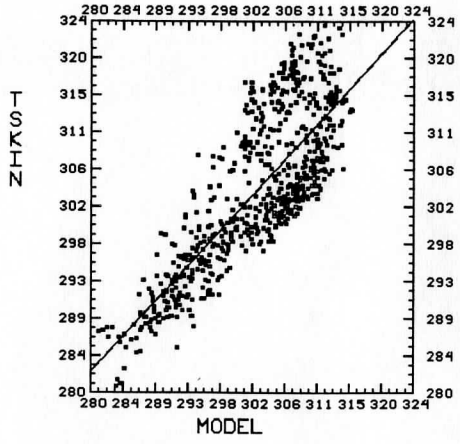
TSKIN
280 284 289 293 298 302 306 311 315 320 324
MODEL

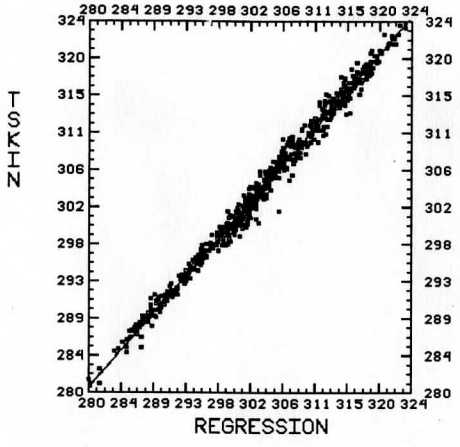
TSKIN
280 284 289 293 298 302 306 311 315 320 324
REGRESSION

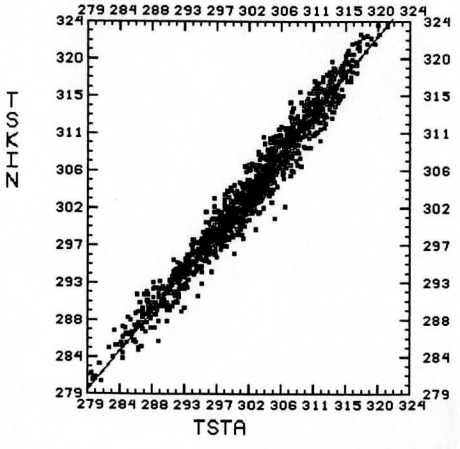
TSKIN
279 284 288 293 297 302 306 311 315 320 324
TSTA

Table 2. Statistical comparison of three methods of obtaining skin temperature estimate; model approximation; air temperature approximation; and regression approximation.

Method	Model	Ta	Regression
mean	-1.27	-1.72	0.13
rms	5.60	2.42	1.59
cc	0.81	0.98	0.99

III. SUMMARY

Over the past year this grant has been a primary source and impetus into the continued development and improvement of satellite-derived products, including their amalgamation into numerical weather prediction models. An example of this evolutionary process is the effort being directed toward initializing forecast models with atmospheric moisture and cloud parameters derived from remotely sensed radiance data. First it was demonstrated that this information can be routinely calculated from the latest version of GOES. Then techniques for incorporating this information into prediction models were developed and shown to improve forecasts on both a coarse and fine scale.

Another step is verifying satellite-derived products on a storm or mesoscale level. This is where the high density surface based observations of VORTEX will be of great value. Comparison and evaluation of satellite sounding products, including temperature and moisture retrievals, relative to the CLASS soundings archived during the intense observation periods of VORTEX will help to further demonstrate the utility of satellite-derived data in the understanding of the storm environment as well as their usefulness in numerical weather prediction models.

As can be seen, support through this contract is important to provide CIMSS researchers the opportunity to perform a wide variety of investigations. Yet, ultimately these studies are focused towards a better understanding of the severe weather forecasting problem.

IV. REFERENCES

Aune, R. M., L. W. Uccellini, R. A. Petersen, and J. J. Tuccillo, 1987: A VAS-numerical model impact study using the Gal-Chen variational approach. *Mon. Wea. Rev.*, **115**, 1010-1035.

*** Aune, R. M., 1994: Improved precipitation predictions using total precipitable water from VAS. *Preprint, Tenth Conference on Numerical Weather Prediction, Amer. Meteor. Soc.,* Portland, OR, 18-22 July, 1994, pp. 192-194.**

Conte, S.D. and C. DeBoor, 1972: Elementary numerical analysis: an algorithm approach. *McGraw-Hill*, New York, 396pp.

Cram, J. M., and M. L. Kaplan, 1985: Variational assimilation of VAS data into a mesoscale model: Assimilation method and sensitivity experiments. *Mon. Wea. Rev.*, **113**, 467-484.

Diak, G. R., D. Kim, M. S. Whipple, and X. Wu, 1992: Preparing for the AMSU. *Bull. Amer. Meteor. Soc.*, **73**, 1009-1035.

Gelfand, I. M., 1963: Calculus of Variations. Prentice-Hall, Inc., New Jersey, 232pp.

*** Hayden, C.M. and R.J. Purser, 1995: Recursive filter objective analysis of meteorological fields, applications to NESDIS Operational Processing. *Jour. Appl. Meteor.*, 34, 3-16.**

*** Hayden, C.M. and Xangquin Wu, 1994: Upper tropospheric relative humidity estimates for GOES. *Preprint Volume, Eighth Conference on Atmospheric Radiance*, Jan 27-28, Nashville, TN, AMS, 58-60.**

*** Herman, L.D., 1993: High frequency satellite cloud motion at high latitudes. *Eighth Symposium on Meteorological Observations and Instrumentation*, Anaheim, CA, Jan. 17-22, 1993.**

*** Herman, L.D. and F.W. Nagle, 1994: A comparison of POES satellite derived winds techniques in the arctic at CIMSS. *Preprint volume, Seventh Conference on Satellite meteorology and Oceanography*, Monterey, CA, June 6-10, 1994.**

Jiang, H-M., and C-H. Shiao, 1989: Numerical experiments of data assimilation using the shallow-water equation model. Papers in *Meteorological Research*, **12**, 33-57.

Kessler, E., 1974: Model of precipitation and vertical air currents. Tellus, **26**, 519-542.

Menzel, W.P. and J.F.W. Purdom, 1994: Introducing GOES-I: The first of a new generation of geostationary operational environmental satellites. *Bull. Amer. Meteor. Soc.*, **75**, 757-781.

Orlanski, I., 1981: The quasi-hydrostatic approximation. *J. Atmos. Sci.*, **38**, 572-582.

Pauley, P.M. and X. Wu, 1994: Reply for comments on "The theoretical, discrete and actual response of the Barnes objective analysis scheme for one- and two-dimensional fields". *Mon. Wea. Rev.*, Vol. **122**, No. 2, 399-401.

*** Rabin, R.M., L.A. McMurdie, C.M. Hayden, and G.S. Wade, 1993: Evaluation of the atmospheric water budget following an intense cold air outbreak over the Gulf of Mexico-Application of a regional forecast model and SSM/I observations. *Jour. Appl. Meteor.*, 32, 3-16.**

Raymond, W. H., and H. L. Kuo, 1982: Simulation of laboratory vortex flow by axisymmetric similarity solutions. *Tellus*, **34**, 588-600.

Raymond, W.H., 1993: Moist wind relationships. *Mon. Wea. Rev.*, **121**, 1992-2003.

*** Raymond, W.H., 1995: Rotationally induced circulations: Equatorial meridional flows. To be submitted to *Dynamics of Atmospheres and Oceans.***

*** Raymond, W.H., 1994: Diffusion and numerical filters. *Mon. Wea. Rev.*, 122, 757-761.**

*** Raymond, W. H., W. S. Olson, G. Callan, 1995: Diabatic forcing and initialization with assimilation of cloud water and rainwater in a forecast model. *Mon. Wea. Rev.*, 123, 366-382.**

*** Schreiner, A. J., D. A. Unger, W. P. Menzel, G. P. Ellrod, K. I. Strabala, and J. L. Pellet, 1993: A comparison of ground and satellite observations of cloud cover. *Bull. Amer. Meteor. Soc.*, 74, 1851-1861.**

Stull, R. B., 1988: An Introduction to Boundary Layer Meteorology. Kluwer Academic Publishers, 666pp.

*** Wu, X., G. R. Diak, C. M. Hayden, 1995: Short-range precipitation forecasts using assimilation of simulated satellite water vapor profiles and column cloud liquid water amounts. *Mon. Wea. Rev.*, 123, 347-365.**

*** Wu, X. and C.M. Hayden, 1995: Variational Assimilation of satellite observed gradient wind in numerical weather prediction. submitted to *Mon. Wea. Rev.***

Zehr, R.M., J.F.W. Purdom, J.F. Weaver, and R.N. Green, 1988: Use of VAS data to diagnose the mesoscale environment of convective storms. *Wea. Forecasting*, **3**, 33-49.

Zhao, Q and T. L. Black, 1994: Implementation of the cloud scheme in the ETA model at NMC. Preprints, 10th Conference on Numerical Weather Prediction, Portland, *Amer. Meteor. Soc.*, 331-332.